Associative electron detachment in sprites

A. Malagón-Romero[1,2], A. Luque[1], Nicholas S. Shuman[3], Thomas M. Miller[4],Shaun G. Ard[3], Albert A. Viggiano[3]

[1]Instituto de Astrofísica de Andalucía (IAA), CSIC, PO Box 3004, Granada 18008, Spain
[2]Centrum Wiskunde and Informatica (CWI), Amsterdam, The Netherlands
[3]Air Force Research Laboratory, Space Vehicles Directorate, Kirtland AFB, New Mexico 87117, USA
[4]Boston College Institute for Scientific Research, Boston, Massachusetts 02549, USA

Key Points:

- Associative detachment of electrons in sprites proceeds almost exclusively from vibrationally excited N_2.
- We provide updated rate coefficients for electron associative detachment.
- In models with the updated rates, sprite glows persist tens of milliseconds, in agreement with observations.

Corresponding author: A. Malagón-Romero, malagon@cwi.nl

Corresponding author: A. Luque, luque@iaa.es

Abstract

The balance of processes affecting electron density drives the dynamics of upper-atmospheric electrical events, such as sprites. We examine the detachment of electrons from negatively charged atomic oxygen (O^-) via collisions with neutral molecular nitrogen (N_2) leading to the formation of nitrous oxide (N_2O). Past research posited that this process, even without significant vibrational excitation of N_2, strongly impacts the dynamics of sprites. We introduce updated rate coefficients derived from recent experimental measurements which suggest a negligible influence of this reaction on sprite dynamics. Given that previous rates were incompatible with the observed persistence times of luminous features in sprites, our findings support that these features result from electron depletion in sprite columns.

Plain Language Summary

Sprites are transient, filamentary luminous structures appearing between approximately 50 and 85 kilometers above Earth's surface. While the primary sprite activity is ephemeral, lasting mere thousandths of a second, certain luminous features persist up to a hundred times longer. The key to understanding these enduring structures lies in the evolution of free electron populations that facilitate electrical conductivity. Here we show that a process that influences this population is slower than previously thought. This may explain why luminous structures can persist for so long.

1 Introduction

Sprites are high-altitude filamentary discharges occurring in the upper mesosphere following a strong cloud-to-ground lightning discharge in a thunderstorm (Pasko et al., 1997; Luque & Ebert, 2009; Liu et al., 2015). One notable benefit arising from the discovery of sprites (Franz et al., 1990) has been a renewed interest in the chemistry of the upper mesosphere, in particular on the reaction mechanisms induced by free, super-thermal electrons as present in sprites, where they are accelerated by intense electric fields. Several questions motivate this interest: for example there is the question of whether sprites have global, regional, or local effects on the composition of the atmosphere (Sentman et al., 2008; Arnone et al., 2008; Gordillo-Vázquez & Pérez-Invernón, 2021; Malagón-Romero et al., 2023). Understanding the spectra of sprites (Gordillo-Vázquez et al., 2012; Passas et al., 2016) is another motivation, particularly relevant in the context of space-based detection of sprites (Chanrion et al., 2019) and discrimination from other events such as Blue Luminous Events (BLUEs) in thundercloud tops (Chanrion et al., 2017; Soler et al., 2020).

Finally, understanding the chemistry of electrons and ions in the upper mesosphere is crucial for elucidating the fundamental physics of sprites. Conversely, investigations into sprites have highlighted previously overlooked reactions. A notable example is the reaction of detachment of electrons from O^- to form N_2O, which is the focus of the present work:

$$O^- + N_2 \longrightarrow N_2O + e. \tag{1}$$

Luque and Gordillo-Vázquez (2012) pointed out that this reaction may strongly affect the dynamics of sprite inception and dynamics. That study questioned the assumption that when the electric field is below a certain, fixed threshold determined by competition between electron impact ionization and electron attachment, free electrons are removed and cease to efficiently transport charge. Detachment reactions such as (1) reverse this attachment and return electrons to their free state. At the time, the most recent laboratory measurements of reaction (1) where those by Rayment and Moruzzi (1978), who argued that the reaction is effective even when nitrogen is in its vibrational ground state. Subsequent studies took for granted the rates of Rayment and Moruzzi (1978) in different contexts. Pancheshnyi (2013) considered how, among others, reaction (1) influences an effective ionization rate whereas da Silva and Pasko (2013) applied them to their investigation of the streamer-to-leader transition.

Other investigations, such as (Luque et al., 2016) indicated potential inaccuracies in the reaction rate coefficients of Rayment and Moruzzi (1978). That study explained the appearance in sprites of

beads and glows, which are luminous structures that persist for up to 100 milliseconds even after the main streamer activity has subsided (Stenbaek-Nielsen & McHarg, 2008). The model presented by Luque et al. (2016) matched the observations but only as long as detachment reactions such as (1) were disregarded. This was later confirmed by Malagón-Romero et al. (2020), where a similar mechanism was proposed as the origin of upward branches in sprites which frequently, if not always, emerge from pre-existing glows.

A further step was taken in a careful literature analysis by Janalizadeh and Pasko (2021), where, besides identifying several issues in the data reporting by Rayment and Moruzzi (1978), they pointed that under atmospheric conditions electron detachment from O^- is not possible in collisions with nitrogen in its ground state.

The controversy motivated Shuman et al. (2023) to carry out new measurements of the reaction rate of (1). The rate coefficients of $O^- + N_2$ were measured using a flow tube apparatus under thermal conditions from 800 K–1200 K; at lower temperatures the rate coefficients were smaller than the limit of the experiment. The results were inconsistent with the literature determination by Rayment and Moruzzi (1978), but supported the results of Janalizadeh and Pasko (2021) indicating that reaction with vibrational ground state N_2 was negligible. The results were modeled and vibrationally resolved rate constants for $v \leq 2$ derived with extrapolation over the thermal range 300 K – 1400 K.

The objective of this study is to investigate the implications of an enhanced understanding of reaction (1) on the chemistry of sprites and related high-atmoshpere electrical phenomena. We hope that this work will garner interest of the geophysical community into the updated knowledge of electron detachment in the atmosphere.

2 Updated reaction rate

As described in detail elsewhere, the $O^- + N_2$ associative detachment reaction must overcome two kinetic bottlenecks. First, a large energetic barrier separates the weakly bound entrance complex $O^-(N_2)$ from the metastable, but longer-lived, N_2O^- intermediate. Second, the system must cross from the N_2O^- anion potential surface to the N_2O neutral potential surface. It happens that both the height of the energetic barrier and the location of the lowest-energy crossing geometry are very similar, about 0.3 eV above the energy of the separated reactants. A simple model considering only the vibrational state of N_2 and the relative kinetic energy of the reactants reproduced the measured thermal rate constants. Increased vibrational energy increased the probability of overcoming the transition state to N_2O^- (both from the inherently higher energy and from increased overlap with the geometry of the transition state, which lies at a larger N-N bond distance). Increased kinetic energy also increased the probability of overcoming the transition state, but decreased the probability of crossing to the neutral surface, such that increasing kinetic energy initially increases the rate coefficient but at larger values decreases the rate coefficient.

The vibrationally-resolved thermal rate constants reported previously are converted to a function of E/n here under the assumption that rotational energy and translational energy affect the reaction similarly (Viggiano & Morris, 1996; Viggiano & Williams, 2001):

$$\frac{E}{n} = \frac{v_d(T_{\text{eff}}, T_0)}{\kappa_0 n_0}, \tag{2}$$

where E/n is the electric field strength divided by neutral gas density, κ_0 is the reduced ion mobility, n_0 is Loschmidt's number, and $v_d(T_{\text{eff}}, T_0)$ is the drift velocity at temperature T_0 equivalent to the thermal velocity at temperature T_{eff} related by

$$v_d(T_{\text{eff}}, T_0) = \left[\frac{3k(T_{\text{eff}} - T_0)}{m_{N_2}}\right]^{1/2}, \tag{3}$$

where k is the Boltzmann constant and m_{N_2} is the nitrogen mass. Here T_0 is taken to be 200 K and T_{eff} are the temperatures reported previously. The values of κ_0 are interpolated from the compilation of Viehland and Mason (1995) up to $E/n = 100$ Td and extrapolated from that data up to 120 Td. Table 1 contains the resulting reaction rate coefficients for reaction (1).

The dependence of the reaction rate coefficients on the effective temperature is well approximated by a modified Arrhenius expression of the form

$$k = k_0 \left(\frac{T_{\text{eff}}}{300\,\text{K}} \right)^d \exp\left(-\frac{T_A}{T_{\text{eff}}} \right). \tag{4}$$

The best-fit parameters k_0, T_A and d for $v = 0, 1, 2$ are listed in table 2. Figure 1 shows the rate coefficients as well as the values from expression (4). Also, as a reasonable approximation that foregoes the use of interpolating tables for the ion mobility, we also show the results of (4) with a constant reduced ion mobility $\kappa_0 = 4.5 \times 10^{-4}\,\text{m}^2\text{V}^{-1}\text{s}^{-1}$. By further neglecting T_0 in (3), we reach this simple expression for the reaction rate coefficient:

$$k = k_0 \left(\frac{E/n}{43\,\text{Td}} \right)^{2d} \exp\left(-\left(\frac{E_A/n}{E/n} \right)^2 \right), \tag{5}$$

with the values of reduced electric fields E_A/n listed in the last column of table 2.

We also plot in figure 1 the reaction rate coefficients by Rayment and Moruzzi (1978) as approximated by Pancheshnyi (2013) (labelled as RM78). For most of the studied range of reduced electric field, the updated rate coefficients for the vibrational ground state of N_2 ($v = 0$) are several orders of magnitude below those from Rayment and Moruzzi (1978). Close to the classical breakdown field ($E/n \approx 120$), the updated rate is still about five times lower than RM78.

3 Implications

We now discuss some of the implications of the new rates on the physics of upper-atmospheric electrical discharges. Table S1 in the supplemental material details a simple chemical scheme that accounts for the main processes within a halo or sprite discharge and up to about 100 ms after its initiation. The rate coefficients for electron-molecule processes, which depend on the electron energy distribution function, are modelled by solving the steady-state Boltzmann equation with the Bolsig+ solver (Hagelaar & Pitchford, 2005) and the Phelps' cross-section database (Phelps & Pitchford, 1985; Lawton & Phelps, 1978) as provided by LxCat (Pancheshnyi et al., 2012; Pitchford et al., 2017; Carbone et al., 2021). With these rates we follow the vibrational distribution of the electronic ground state of nitrogen, which induce associative detachment from O^- with the rates discussed in the previous section. We also consider detachment from $O_2{}^-$ and negative ion conversion as modelled by Pancheshnyi (2013). Finally, for the sake of completeness, we include positive ion conversion as modelled by Aleksandrov and Bazelyan (1999) and electron-ion and ion-ion recombination as modelled by Kossyi et al. (1992).

To compare with previous models, we also consider a reaction scheme where the rate of (1) follows Rayment and Moruzzi (1978) as fitted by Pancheshnyi (2013) and regardless of the vibrational state of N_2. We name the two models "new" and "RM78".

First we look at the chemical evolution under constant reduced electric field. Figure 2 shows the evolution of the main negatively-charged species in the wake of a streamer that leaves an electron density $n_e = 10^{11}\,\text{m}^{-3}$ at an altitude of 80 km. The left column of the figure (labelled (a)) corresponds to the reaction rates of (1) presented here, whereas the right column (b) contains the densities predicted by the rates by Rayment and Moruzzi (1978). In both cases we simulate constant applied reduced electric fields of 70 Td and 90 Td.

There are clear differences between the two columns. Enhanced detachment rates of O^- in the right column result in elevated electron and O^- densities. Specifically, at an electric field strength of 70 Td with the updated rate coefficients, the electron density exhibits a two-order-of-magnitude reduction prior to stabilization. In contrast, according to the rate coefficients of Rayment and Moruzzi (1978), the electron density experiences only a marginal decrease before entering a growth regime.

Next we investigate the consequences of the updated reaction rate coefficient in a self-consistent 2D axisymmetric model of a sprite discharge. In this model, the electron density (n_e) under a local

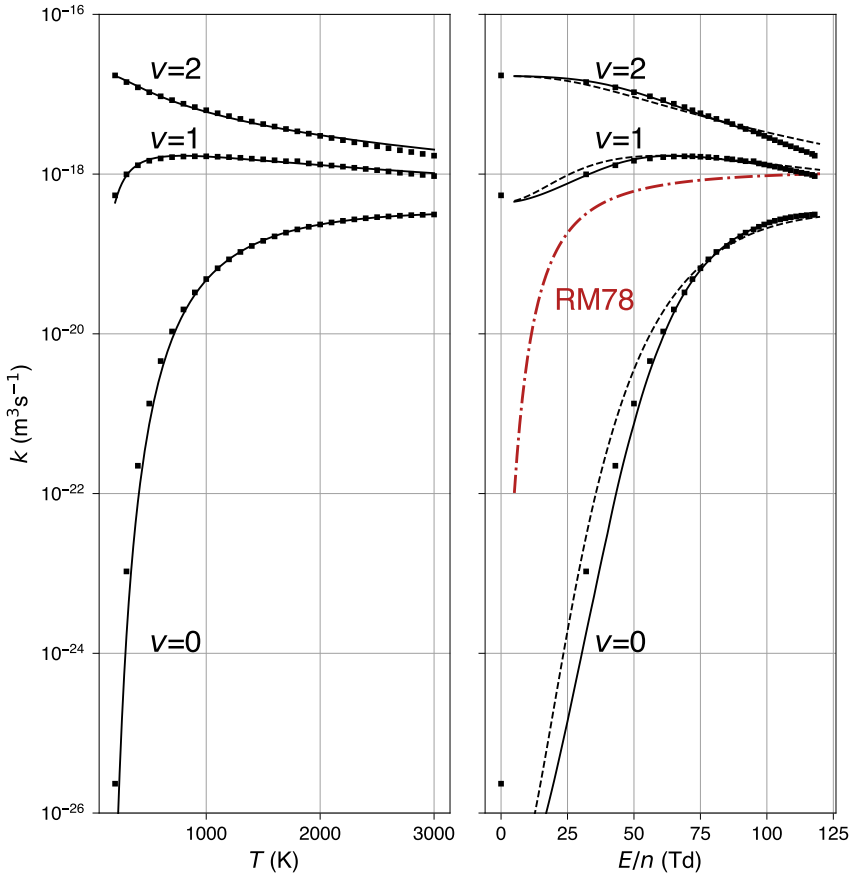

Figure 1. Rate coefficients of $O^- + N_2(v) \longrightarrow N_2O + e$ for $v = 0, 1, 2$. On the left panel we show the dependence of the rate coefficients on temperature assuming equilibrium conditions. The dots correspond to the values in table 1 whereas lines show the fits using (4) with the parameters listed in table 2. The right panel shows the rate dependence on the reduced electric field, following the conversion of equations (2) and (3) with $T_0 = 200\,\mathrm{K}$. The solid lines use the same fits as in the left panel and the ion mobilities from Viehland and Mason (1995). The dashed lines replace these mobilities by a field-independent reduced ion mobility $\kappa_0 = 4.5 \times 10^{-4}\,\mathrm{m^2V^{-1}s^{-1}}$.

Table 1. Reaction rate coefficients for the reaction $O^- + N_2(v) \longrightarrow N_2O + e$ for different values of an effective collision temperature T_{eff} and reduced electric field E/n. K_0 is the mobility of O^- ions for the given electric field, at atmospheric pressure and 300 K. For drift velocities below 10^3 ms^{-1} (reduced electric fields below $E/n \approx 85$ Td) we use ion mobilities interpolated from Viehland and Mason (1995) for higher reduced electric fields we extrapolate as $K_0 = 1 \times 10^{-4}\,\text{m}^2\text{V}^{-1}\text{s}^{-1} \times \ln(v_d(T_{\text{eff}})/10^{-2}\,\text{ms}^{-1}) - 7 \times 10^{-4}\,\text{m}^2\text{V}^{-1}\text{s}^{-1}$.

T_{eff}(K)	E/n (Td)	K_0 (m^2 V^{-1} s^{-1})	k (m^3 s^{-1})		
			v=0	v=1	v=2
200	0	3.33×10^{-4}	2.33×10^{-26}	5.42×10^{-19}	1.72×10^{-17}
300	32	3.5×10^{-4}	1.06×10^{-23}	9.93×10^{-19}	1.42×10^{-17}
400	43	3.67×10^{-4}	2.23×10^{-22}	1.29×10^{-18}	1.22×10^{-17}
500	50	3.81×10^{-4}	1.34×10^{-21}	1.47×10^{-18}	1.06×10^{-17}
600	56	3.94×10^{-4}	4.56×10^{-21}	1.57×10^{-18}	9.42×10^{-18}
700	61	4.06×10^{-4}	1.07×10^{-20}	1.63×10^{-18}	8.43×10^{-18}
800	65	4.17×10^{-4}	2.02×10^{-20}	1.66×10^{-18}	7.60×10^{-18}
900	69	4.27×10^{-4}	3.30×10^{-20}	1.67×10^{-18}	6.90×10^{-18}
1000	72	4.35×10^{-4}	4.85×10^{-20}	1.67×10^{-18}	6.30×10^{-18}
1100	75	4.43×10^{-4}	6.62×10^{-20}	1.65×10^{-18}	5.78×10^{-18}
1200	78	4.5×10^{-4}	8.56×10^{-20}	1.63×10^{-18}	5.32×10^{-18}
1300	81	4.55×10^{-4}	1.06×10^{-19}	1.60×10^{-18}	4.91×10^{-18}
1400	83	4.56×10^{-4}	1.26×10^{-19}	1.56×10^{-18}	4.55×10^{-18}
1500	86	4.59×10^{-4}	1.46×10^{-19}	1.53×10^{-18}	4.23×10^{-18}
1600	89	4.62×10^{-4}	1.66×10^{-19}	1.49×10^{-18}	3.94×10^{-18}
1700	91	4.66×10^{-4}	1.85×10^{-19}	1.45×10^{-18}	3.67×10^{-18}
1800	94	4.69×10^{-4}	2.03×10^{-19}	1.45×10^{-18}	3.43×10^{-18}
1900	96	4.72×10^{-4}	2.19×10^{-19}	1.36×10^{-18}	3.21×10^{-18}
2000	99	4.75×10^{-4}	2.34×10^{-19}	1.32×10^{-18}	3.01×10^{-18}
2100	102	4.78×10^{-4}	2.48×10^{-19}	1.28×10^{-18}	2.83×10^{-18}
2200	105	4.8×10^{-4}	2.60×10^{-19}	1.24×10^{-18}	2.66×10^{-18}
2300	107	4.83×10^{-4}	2.71×10^{-19}	1.20×10^{-18}	2.50×10^{-18}
2400	110	4.85×10^{-4}	2.80×10^{-19}	1.16×10^{-18}	2.36×10^{-18}
2500	113	4.87×10^{-4}	2.89×10^{-19}	1.12×10^{-18}	2.23×10^{-18}
2600	117	4.89×10^{-4}	2.95×10^{-19}	1.08×10^{-18}	2.11×10^{-18}
2700	120	4.91×10^{-4}	3.01×10^{-19}	1.04×10^{-18}	1.99×10^{-18}
2800	123	4.93×10^{-4}	3.06×10^{-19}	1.01×10^{-18}	1.89×10^{-18}
2900	127	4.95×10^{-4}	3.09×10^{-19}	9.77×10^{-19}	1.79×10^{-18}
3000	131	4.97×10^{-4}	3.12×10^{-19}	9.44×10^{-19}	1.70×10^{-18}

Table 2. Fitting parameters for the reaction rate coefficients for the reaction $O^- + N_2(v) \longrightarrow N_2O + e$ with $v = 0, 1, 2$ according to expression 4.

v	k_0 (m^{3}s^{-1})	T_A (K)	d	E_A/n (Td)
0	3.98×10^{-17}	5097	-1.36	176
1	9.04×10^{-18}	674	-0.85	64
2	2.74×10^{-17}	186	-1.10	34

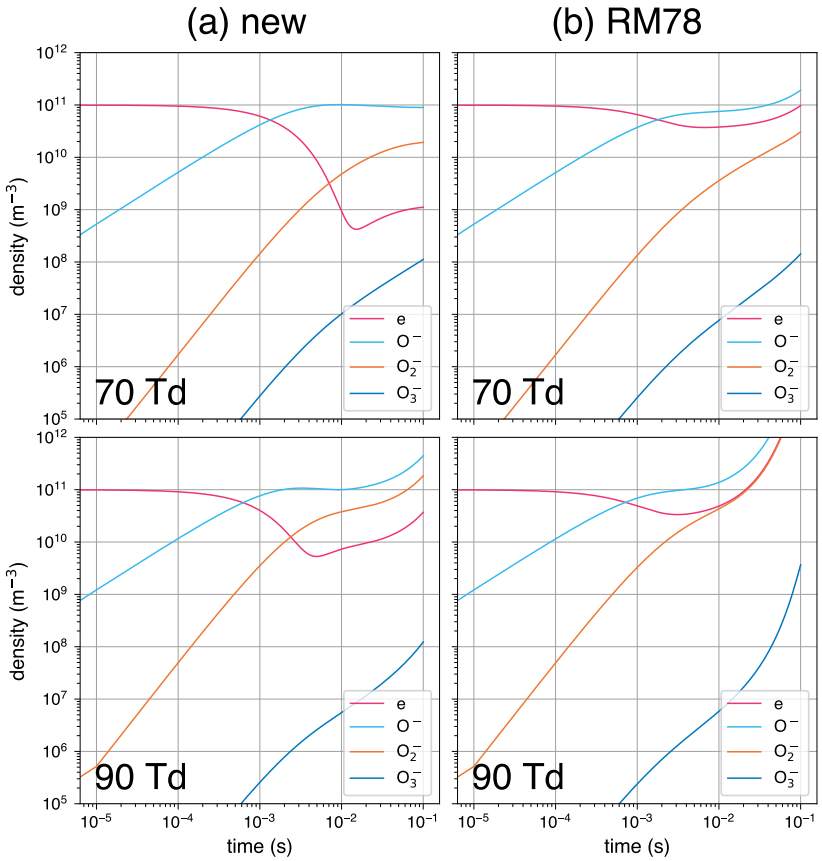

Figure 2. Evolution of the dominant negatively-charged species in our chemical models under a constant reduced electric field. Starting with an initial condition of an electron density of 10^{11} m^{-3}, which is representative of the state of a sprite column in the wake of a streamer at 80 km.

electric field $\boldsymbol{E}$, evolves according to the conservation equation:

$$\partial_t n_e = \nabla \cdot (\mu_e \boldsymbol{E} + D_e \nabla n_e) + C_e, \tag{6}$$

where μ_e and D_e are the electron mobility and the diffusion coefficient, and C_e is the chemical source term accounting for the chemical reactions listed in table S1 in the supplemental material. Transport coefficients (μ_e and D_e) are assumed to be functions of the local electric field and are computed with Bolsig+ (Hagelaar & Pitchford, 2005) using as above the cross sections for electron impact with N_2 and O_2 provided in Phelps' database retrieved from LxCat.

Neutral species and ions (n_i with $i = 0, 1, ...$) are considered motionless and their time evolution obeys a simplified version of equation (6), namely,

$$\partial_t n_i = C_i, \tag{7}$$

where C_i is the chemical source term determined by the reactions in table S1 in the supplemental material.

The electric field $\boldsymbol{E}$, is calculated as $\boldsymbol{E} = -\nabla\phi$, where ϕ is the electrostatic potential obtained upon the solution of Poisson's equation

$$\nabla^2\phi = \sum_s \frac{q_s n_s}{\varepsilon_0}, \tag{8}$$

where the sum extends over all charged species s, q_s is the charge of the species s and ε_0 is the vacuum permittivity.

The model is implemented in Afivo-streamer (Teunissen & Ebert, 2017) and is based on Afivo (Teunissen & Ebert, 2018), an octree-based adaptive mesh refinement framework, with OpenMP capabilities and a geometric multigrid solver for Poisson's equation. Equations (6) and (7) are solved with an explicit second order time stepping and a flux-limited second order accurate spatial discretization.

In this study, we initiate our model with the exact same conditions discussed by Malagón-Romero et al. (2020), that consist in a neutral column of radius $a_0 = 400\,\mathrm{m}$ with a truncated funnel attached to its lower part that roughly approximates the multiple branching events the parent streamer discharge undergoes as it propagates. The initial electron density is then computed as

$$n_\mathrm{e}(r, z) = n_{\mathrm{e},0}\,(z)\,\frac{a_0^2}{a\,(z)}\,\max\left(0, 1 - \frac{r^2}{a\,(z)^2}\right) + n_{\mathrm{e,bg}}(z), \tag{9}$$

where $n_{\mathrm{e},0}(z) = C n_\mathrm{air}\,(z)$ is the electron density at the axis, $C = 3.33 \times 10^{-11}$, n_air is the air density obtained by scaling the ground air density $n_{\mathrm{air},0} = 2.5 \times 10^{25}\,\mathrm{m}^{-3}$ as $n_\mathrm{air}(z) = n_{\mathrm{air},0}\exp(-z/7.2\,\mathrm{km})$, and $a(z)$ is a piece-wise linear function that models the radius of the channel and the funnel, ensuring a smooth transition. The funnel has a radius of 5 km at the base $z_\mathrm{b} = 50\,\mathrm{km}$ with the upper vertex at $z_\mathrm{u} = 60\,\mathrm{km}$ and is calculated as

$$a(z) = \max\left(a_0, \frac{z_\mathrm{u} - z}{z_\mathrm{u} - z_\mathrm{b}} \times 5\,\mathrm{km}\right). \tag{10}$$

Finally, the background electron density follows the Wait-Spies profile estimated by Hu et al. (2007):

$$n_{\mathrm{e,bg}}(z) = 10^{-2}\,\mathrm{cm}^{-3}\exp\left(-\frac{z - 60\,\mathrm{km}}{2.86\,\mathrm{km}}\right). \tag{11}$$

The computational domain is a 10 km radius and 40 km height cylinder with its base at 40 km altitude. The minimum grid spacing in our simulation has been 1.22 m. We apply homogeneous Neumann boundary conditions at all boundaries to solve equations (6) and (7). Poisson's equation has been solved with homogeneous Neumann boundary conditions at the axis and outer boundaries. The bottom boundary is grounded while the top boundary is set to a fixed voltage of 2.9 MV. The

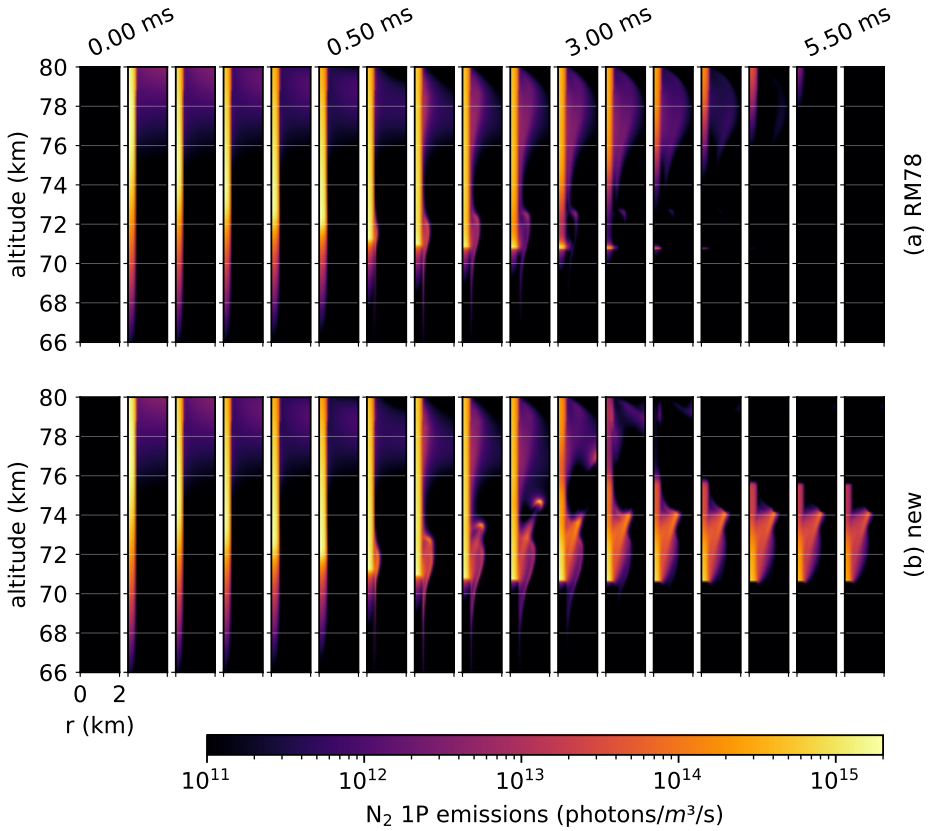

Figure 3. Modeled light emissions from a sprite column. Both for the reaction rate coefficients by (Rayment & Moruzzi, 1978) (upper row) and the updated reaction rate coefficients in table 1 (lower row), we show the instantaneous emissions of photons from the first positive system of molecular nitrogen (N2 1P). The snapshots are taken at intervals of 0.1 ms up to 0.5 ms and of 0.5 ms afterwards.

result is a constant background field of 72.38 V/m pointing downwards, setting a reduced electric field E/n_{air} of approximately 120 Td at roughly 77 km.

The results are displayed in figure 3 where we show simulated light emissions (N2 1P) from the sprite column. With the detachment rate coefficients of Rayment and Moruzzi (1978) (RM78) a more elevated conductivity inside the column contributes to a fast screening of the electric field and light emissions that decay within a few milliseconds. On the other hand, with the updated rates of detachment (new), the attachment instability discussed e.g. by Luque et al. (2016) leads to a sharply defined, light-emitting segment which is consistent with observations (Stenbaek-Nielsen & McHarg, 2008; Bór, 2013).

A closer look at the light-emitting segment in figure 4 shows that the luminosity decays faster than exponentially within 5 ms when using the RM78 detachment rate coefficients. This contrasts with the results for the new detachment rate coefficients (table 1). In this case, the luminosity exhibits an exponential decay, consistent with observations (Luque et al., 2016), with a decay constant of approximately 1.7 ms. The exponential trend becomes evident after 6 ms, whereas observations show it almost from the very beginning. This discrepancy is likely attributed to the neutral charge conditions used to initiate the simulations.

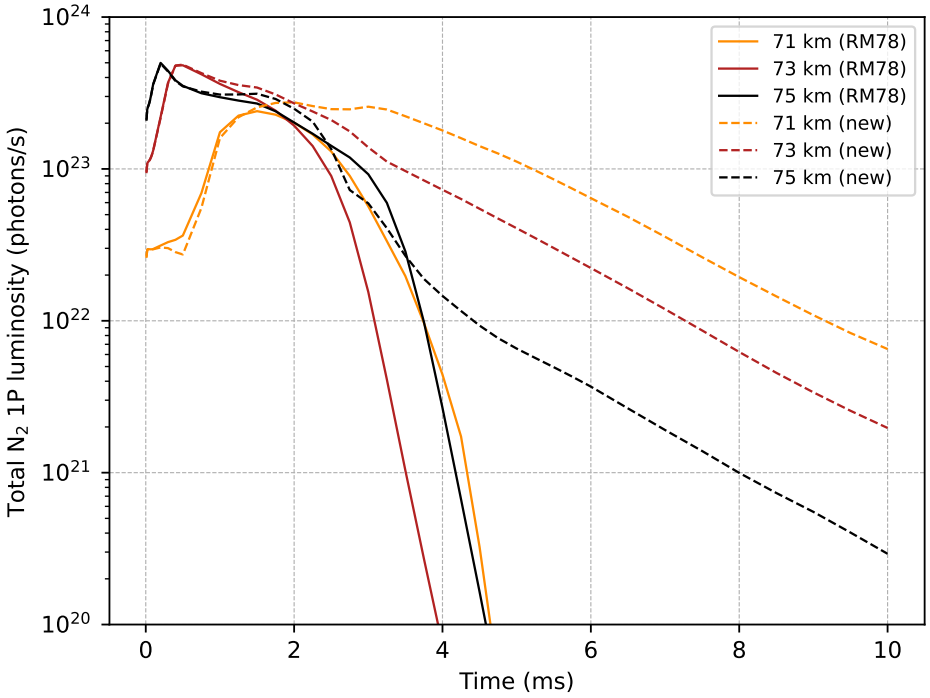

Figure 4. Emissions from the first positive system of N_2 integrated in 400 m-radius and 1 km-tall cylinders centered at 71 km, 73 km and 75 km altitudes, considering the detachment rate coefficient from Rayment and Moruzzi (1978) (RM78) and the updated detachment rate coefficients from table 1 (new), showing faster than exponential and exponential decay respectively.

4 Conclusions

In this work we provide updated rate coefficients for the reaction of associative electron detachment and discuss its implications for the dynamics of sprites. For the vibrational ground state of N_2, these rate are significantly smaller than previous estimates. We conclude that, given the low population of vibrationally excited N_2, this reaction is too slow to play a significant role in sprites.

Future investigations of electrical phenomena in the upper atmosphere should consider the new understanding of electron associative detachment presented here. For relatively short timescales such as those of sprites the reaction process can be disregarded. The possibility that it is relevant for timescales beyond the tens of milliseconds deserves to be studied in the future.

Open Research Section

The code containing the simple sprite chemical model used to generate figure 2 is available in the repository `https://github.com/aluque/spritechem` (hash `aceaced`...). The output and source files for the generation of the results presented in figures 3 and 4 are openly available at `https://doi.org/10.5281/zenodo.10219918`.

Acknowledgments

A. Malagón-Romero and A. Luque acknowledge financial support from the Spanish Ministry of Science and Innovation, under project PID2022-136348NB-C31 and from the State Agency for Research of the Spanish MCIU through the "Center of Excellence Severo Ochoa" award for the Instituto de Astrofísica de Andalucía (CEX2021-001131-S). A. Malagón-Romero acknowledges the financial support from the grants BEVP34S12931 and BEVP34A6840 funded by "Ramón Areces Foundation".

The AFRL work is supported by the Air Force Office of Scientific Research for support under AFOSR-22RVCOR009. TMM is supported through the Institute for Scientific Research of Boston College under contract No. FA9453-20-C-0048. We thank Reza Janalizadeh for bringing the questions concerning the associative detachment to our attention.

The views expressed are those of the authors and do not reflect the official guidance or position of the Department of the Air Force, the Department of Defense (DoD), or the United States government. The appearance of external hyperlinks does not constitute endorsement by the United States DoD of the linked websites, or the information, products, or services contained therein. The DoD does not exercise any editorial, security, or other control over the information you may find at these locations.

References

Aleksandrov, N. L., & Bazelyan, E. M. (1999). Ionization processes in spark discharge plasmas. *Plasma Sour. Sci. Technol.*, *8*(2), 285. doi: 10.1088/0963-0252/8/2/309

Arnone, E., Kero, A., Dinelli, B. M., Enell, C. F., Arnold, N. F., Papandrea, E., ... Turunen, E. (2008). Seeking sprite-induced signatures in remotely sensed middle atmosphere NO_2. *Geophys. Res. Lett.*, *35*(5), L05807. doi: 10.1029/2007GL031791

Bór, J. (2013). Optically perceptible characteristics of sprites observed in Central Europe in 2007-2009. *J. Atm. Sol.-Terr. Phys.*, *92*, 151-177. doi: 10.1016/j.jastp.2012.10.008

Carbone, E., Graef, W., Hagelaar, G., Boer, D., Hopkins, M. M., Stephens, J. C., ... LXCat Team (2021). Data Needs for Modeling Low-Temperature Non-Equilibrium Plasmas: The LXCat Project, History, Perspectives and a Tutorial. *Atoms*, *9*(1), 16. doi: 10.3390/atoms9010016

Chanrion, O., Neubert, T., Lundgaard Rasmussen, I., Stoltze, C., Tcherniak, D., Jessen, N. C., ... Lorenzen, M. (2019). The Modular Multispectral Imaging Array (MMIA) of the ASIM Payload on the International Space Station. *Space Sci. Rev.*, *215*(4), 28. doi: 10.1007/s11214-019-0593-y

Chanrion, O., Neubert, T., Mogensen, A., Yair, Y., Stendel, M., Singh, R., & Siingh, D. (2017). Profuse activity of blue electrical discharges at the tops of thunderstorms. *Geophys. Res. Lett.*, *44*(1), 496-503. doi: 10.1002/2016GL071311

da Silva, C. L., & Pasko, V. P. (2013). Dynamics of streamer-to-leader transition at reduced air densities and its implications for propagation of lightning leaders and gigantic jets. *J. Geophys. Res. (Atmos.)*, *118*(24), 13,561-13,590. doi: 10.1002/2013JD020618

Franz, R. C., Nemzek, R. J., & Winckler, J. R. (1990). Television Image of a Large Upward Electrical Discharge Above a Thunderstorm System. *Science*, *249*(4964), 48-51. doi: 10.1126/science.249.4964.48

Gordillo-Vázquez, F. J., Luque, A., & Simek, M. (2012). Near infrared and ultraviolet spectra of TLEs. *J. Geophys. Res. (Space Phys)*, *117*(A5), A05329. doi: 10.1029/2012JA017516

Gordillo-Vázquez, F. J., & Pérez-Invernón, F. J. (2021). A review of the impact of transient luminous events on the atmospheric chemistry: Past, present, and future. *Atmospheric Research*, *252*, 105432. doi: 10.1016/j.atmosres.2020.105432

Hagelaar, G. J. M., & Pitchford, L. C. (2005). Solving the Boltzmann equation to obtain electron transport coefficients and rate coefficients for fluid models. *Plasma Sour. Sci. Technol.*, *14*(4), 722-733. doi: 10.1088/0963-0252/14/4/011

Hu, W., Cummer, S. A., & Lyons, W. A. (2007). Testing sprite initiation theory using lightning measurements and modeled electromagnetic fields. *J. Geophys. Res. (Atmos.)*, *112*(D13), D13115. doi: 10.1029/2006JD007939

Janalizadeh, R., & Pasko, V. P. (2021). Implications of Electron Detachment in Associative Collisions of Atomic Oxygen Anion with Molecular Nitrogen for Modeling of Transient Luminous Events. *Geophys. Res. Lett.*, *48*(4), e91134. doi: 10.1029/2020GL091134

Kossyi, I. A., Kostinsky, A. Y., Matveyev, A. A., & Silakov, V. P. (1992). Kinetic scheme of the non-equilibrium discharge in nitrogen-oxygen mixtures. *Plasma Sour. Sci. Technol.*, *1*(3), 207-220. doi: 10.1088/0963-0252/1/3/011

Lawton, S. A., & Phelps, A. V. (1978). Excitation of the $b^1\Sigma_g^+$ state of O_2 by low energy electrons. *J. Chem. Phys.*, *69*, 1055. doi: 10.1063/1.436700

Liu, N., McHarg, M. G., & Stenbaek-Nielsen, H. C. (2015). High-altitude electrical discharges associated with thunderstorms and lightning. *J. Atm. Sol.-Terr. Phys.*, *136*, 98-118. doi: 10.1016/j.jastp.2015.05.013

Luque, A., & Ebert, U. (2009). Emergence of sprite streamers from screening-ionization waves in the lower ionosphere. *Nature Geoscience*, *2*(11), 757-760. doi: 10.1038/ngeo662

Luque, A., & Gordillo-Vázquez, F. J. (2012). Mesospheric electric breakdown and delayed sprite ignition caused by electron detachment. *Nature Geoscience*, *5*(1), 22-25. doi: 10.1038/ngeo1314

Luque, A., Stenbaek-Nielsen, H. C., McHarg, M. G., & Haaland, R. K. (2016). Sprite beads and glows arising from the attachment instability in streamer channels. *J. Geophys. Res. (Space Phys)*, *121*(3), 2431-2449. doi: 10.1002/2015JA022234

Malagón-Romero, A., Pérez-Invernón, F. J., & Gordillo-Vázquez, F. J. (2023). Chemical Activity of Low Altitude (50 km) Sprite Streamers. *J. Geophys. Res. (Atmos.)*, *128*(14), e2023JD038570. doi: 10.1029/2023JD038570

Malagón-Romero, A., Teunissen, J., Stenbaek-Nielsen, H. C., McHarg, M. G., Ebert, U., & Luque, A. (2020). On the Emergence Mechanism of Carrot Sprites. *Geophys. Res. Lett.*, *47*(1), e85776. doi: 10.1029/2019GL085776

Pancheshnyi, S. (2013). Effective ionization rate in nitrogen-oxygen mixtures. *J. Phys. D*, *46*(15), 155201. doi: 10.1088/0022-3727/46/15/155201

Pancheshnyi, S., Biagi, S., Bordage, M. C., Hagelaar, G. J. M., Morgan, W. L., Phelps, A. V., & Pitchford, L. C. (2012). The LXCat project: Electron scattering cross sections and swarm parameters for low temperature plasma modeling. *Chem. Phys.*, *398*, 148-153. doi: 10.1016/j.chemphys.2011.04.020

Pasko, V. P., Inan, U. S., Bell, T. F., & Taranenko, Y. N. (1997). Sprites produced by quasi-electrostatic heating and ionization in the lower ionosphere. *J. Geophys. Res.*, *102*(A3), 4529-4562. doi: 10.1029/96JA03528

Passas, M., Sánchez, J., Sánchez-Blanco, E., Luque, A., & Gordillo-Vázquez, F. J. (2016). a

spectrograph for the study of transient luminous events. *App. Optics*, *55*(23), 6436. doi: 10.1364/AO.55.006436

Phelps, A. V., & Pitchford, L. C. (1985). Anisotropic scattering of electrons by N_2 and its effect on electron transport. *Phys. Rev. A*, *31*(5), 2932-2949. doi: 10.1103/PhysRevA.31.2932

Pitchford, L. C., Alves, L. L., Bartschat, K., Biagi, S. F., Bordage, M.-C., Bray, I., ... Pancheshnyi, S. (2017). Lxcat: an open-access, web-based platform for data needed for modeling low temperature plasmas. *Plasma Processes and Polymers*, *14*(1-2), 1600098. doi: https://doi.org/10.1002/ppap.201600098

Rayment, S. W., & Moruzzi, J. L. (1978). Electron detachment studies between O- ions and nitrogen. *Int. J. Mass Spectrom. Ion Processes*, *26*(3), 321-326. doi: 10.1016/0020-7381(78)80033-3

Sentman, D. D., Stenbaek-Nielsen, H. C., McHarg, M. G., & Morrill, J. S. (2008). Plasma chemistry of sprite streamers. *J. Geophys. Res. (Atmos.)*, *113*(D11), D11112. doi: 10.1029/2007JD008941

Shuman, N. S., Miller, T. M., Ard, S. G., & Viggiano, A. A. (2023). Kinetics of associative detachment of O^- + N_2 and dissociative attachment of e^- + N_2O up to 1300 K. *Phys. Chem. Chem. Phys.*. ((in press))

Soler, S., Pérez-Invernón, F. J., Gordillo-Vázquez, F. J., Luque, A., Li, D., Malagón-Romero, A., ... Østgaard, N. (2020). Blue optical observations of narrow bipolar events by asim suggest corona streamer activity in thunderstorms. *Journal of Geophysical Research: Atmospheres*, *125*(16), e2020JD032708. doi: 10.1029/2020JD032708

Stenbaek-Nielsen, H. C., & McHarg, M. G. (2008). High time-resolution sprite imaging: observations and implications. *J. Phys. D*, *41*(23), 234009. doi: 10.1088/0022-3727/41/23/234009

Teunissen, J., & Ebert, U. (2017). Simulating streamer discharges in 3D with the parallel adaptive Afivo framework. *J. Phys. D*, *50*(47), 474001. doi: 10.1088/1361-6463/aa8faf

Teunissen, J., & Ebert, U. (2018). Afivo: A framework for quadtree/octree AMR with shared-memory parallelization and geometric multigrid methods. *Comput. Phys. Commun.*, *233*, 156-166. doi: 10.1016/j.cpc.2018.06.018

Viehland, L. A., & Mason, E. A. (1995). Transport Properties of Gaseous Ions over a Wide Energy Range, Part IV. *At. Data Nucl. Data Tables*, *60*, 37. doi: 10.1006/adnd.1995.1004

Viggiano, A. A., & Morris, R. A. (1996). Rotational and vibrational energy effects on ion-molecule reactivity as studied by the vt-sifdt technique. *J. Phys. Chem.*, *100*(50), 19227-19240. Retrieved from `https://doi.org/10.1021/jp962084x` doi: 10.1021/jp962084x

Viggiano, A. A., & Williams, S. (2001). Rotational and vibrational energy effects on ion-molecule reactivity as studied by VT-SIFDT technique. In L. M. Babcock & N. G. Adams (Eds.), *Advances in gas phase ion chemistry* (Vol. 4, pp. 85–136). Elsevier.